

Supplement of Atmos. Chem. Phys., 18, 1241–1262, 2018
<https://doi.org/10.5194/acp-18-1241-2018-supplement>
© Author(s) 2018. This work is distributed under
the Creative Commons Attribution 3.0 License.



Supplement of

The early summertime Saharan heat low: sensitivity of the radiation budget and atmospheric heating to water vapour and dust aerosol

Netsanet K. Alamirew et al.

Correspondence to: Netsanet K. Alamirew (na286@sussex.ac.uk) and Martin C. Todd (m.todd@sussex.ac.uk)

The copyright of individual parts of the supplement might differ from the CC BY 3.0 License.

SUPPLEMENTARY MATERIAL

S1 Optical Properties of dust

SSA values in the band covering the spectral range 0.32 to 0.69 μm are 0.82 and 0.91 for Fennec-Ryder and Dubovik respectively. The coarser particles in Fennec-Ryder result in a lower SSA – i.e. more absorbing dust. Note that in the model since AOD is fixed based on the observed AOD, the vertical profile of dust mass mixing ratio is adjusted so that when combined with the MEC shown in fig. 5 (main paper), the AOD in the spectral range 0.32 to 0.69 μm is correct. Therefore the differences in MEC between the two datasets shown in fig. 5 cannot result in differences within the RT model. However, differences in SSA and g are able to exert different impacts on the radiative fluxes within the RT model, as described in section 4.

S2 RT Sensitivity experiments to choice of inputs

For some quantities, we do not have direct observations so we use alternative data from various sources. In the ‘configuration mode’ we test the uncertainty of the modelled radiative fluxes to uncertainties in these model inputs using the experiments summarised in Table S1. Then comparison of TOA fluxes with satellite observation allows us to arrive at what we consider to be an ‘optimal’ model configuration for the subsequent model ‘experiment mode’ analysis.

(i) Surface skin temperature. Since there are no complete observations of skin temperature we use reanalysis products as inputs to the RT code and we use both these data to further investigate sensitivity of flux to uncertainty in skin temperature. Figure 6 displays the time series of surface skin temperature from ERA-I, MERRA, and CERES footprint data. Root mean square difference (RMSD) of the reanalysis products with respect to CERES-footprint data are high (4.5 K and 5.5 K for MERRA and ERA-I, respectively). Fig. S1 further confirms that MERRA has strong diurnal anomalies compared with ERA-I. Despite the higher RMSD of ERA-I skin temperature compared with RMSD of MERRA, the RMSD of ERA-I 2 m air temperature (Figure 6) with respect to flux tower measurement is 3.1 K (3.7 K, MERRA). The relatively bigger RMSD in skin temperature could be due to the uncertainty in CERES measurements.

(ii) Surface emissivity. We test the sensitivity of radiative fluxes to uncertainty in estimates of surface emissivity using CERES measurements and MERRA outputs that have monthly mean values of 0.89 and 0.94 respectively.

(iii) Surface albedo. We noted that in contrast to observations the reanalysis products have weak representation of the diurnal cycle in surface albedo (Figure 3). Although we use observed surface albedo throughout all our experiment model RT runs, we also test the sensitivity of TOA shortwave flux to reanalysis surface albedo errors.

(iv) Dust Size Distribution. We test sensitivity of dust radiative forcing to the two size distribution described in the paper, Dubovik dust and Fennec-Ryder dust. Comparison of TOA direct radiative effect of dust with measurements and previous published results are used as basis for the choice of size distribution of dust. The results of sensitivity of radiative flux to dust size distributions is provided in the paper.

(iv) Cloud Properties. Acquiring observations of the vertical structure of clouds of sufficient quality for radiative transfer calculations is always challenging. Here we use the ERA-I and MERRA outputs of cloud fraction, liquid and ice water mixing ratios. Cloud is treated to have maximum overlap in a column where ice and

water are mixed homogeneously. During the Fennec period, cloud was characterised by shallow cumulus or altocumulus near the top of the PBL and occasional deep convection. It is likely that the relatively coarse vertical and horizontal resolution of both reanalysis models will have considerable bias and we recognise that this is likely to underestimate the true cloud-related uncertainty, and for example, M16 suggest that ERA-I underestimate cloud fraction by a factor of 2.5.

S3 RT model optimum configuration

Sensitivity of RT simulated fluxes to uncertainty in the surface skin temperature and emissivity is low compared to the sensitivity to other factors (Table S1) with variations of $\sim 2 \text{ W m}^{-2}$ at TOA and $5\text{-}6 \text{ W m}^{-2}$ at surface. Based on bias with respect to CERES-EBFA observations we use ERA-I skin temperature and MERRA emissivity products for the ‘optimal’ configuration.

TOA fluxes are not strongly sensitive to the choice of cloud properties with TOA net flux variations of $\sim 4 \text{ W m}^{-2}$. On the basis of bias with respect to observations we select the ERA-I cloud properties. It should however be noted that reanalysis is likely to have problems resolving the type of cloud over Sahara i.e. shall, shallow top of boundary layer cumulus. It is interesting to note that TOA radiative fluxes are quite sensitive to the errors in surface albedo from reanalysis with differences up to 16 W m^{-2} compared to the optimum configuration, which used observed surface albedo. This suggests that it is important to have good observational data, which captures the strong diurnal cycle of surface albedo to achieve accurate radiative fluxes.

Table S1. Summary of model configuration mode sensitivity analysis

Sensitivity input variable	Source of data for sensitivity run	Sensitivity results	‘Optimal configuration choice
surface albedo	Fennec measured quantity versus ERA-I	Difference of upto 16 W m^{-2} in TOA net SW flux	Surface Albedo calculated from surface flux measurements
skin temperature	ERA-I MERRA	Difference of 6 W m^{-2} in surface net LW flux	ERA-I skin temperature estimate
Surface emissivity	CERES MERRA	Differences of 2.3 W m^{-2} at TOA LW flux and 5 W m^{-2} at the surface.	MERRA reanalysis estimates
Cloud fraction and mixing ratio	ERA-I MERRA	Difference of 4 W m^{-2} both at TOA and surface net SW flux	ERA-I
dust size distribution	Dubovik FENNEC-Ryder	TOA SW dust DRE -2 W m^{-2} Using Dubovik and 23 W m^{-2} using Ryder-FENNEC	Dubovik

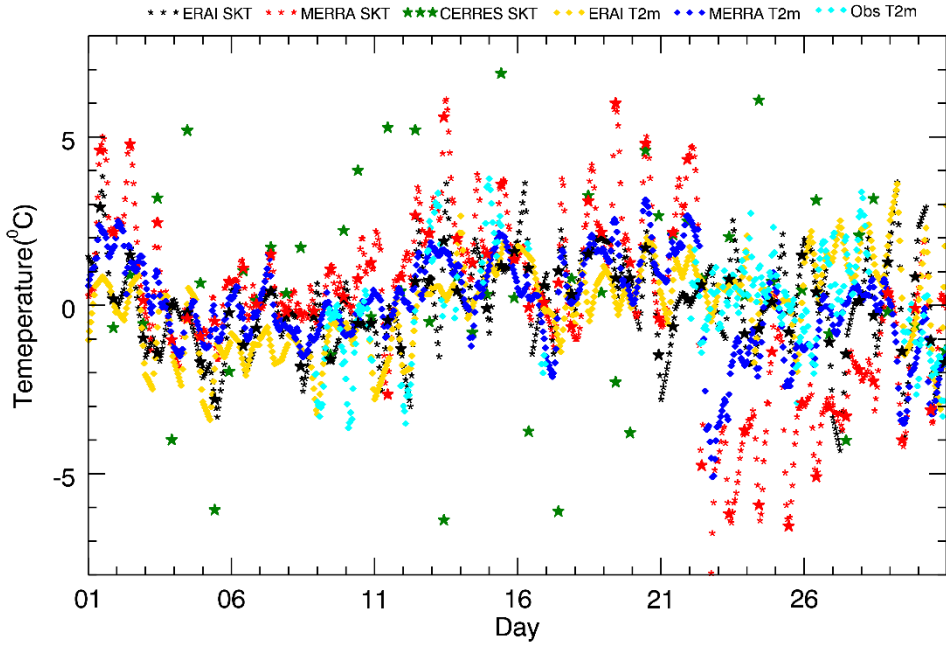
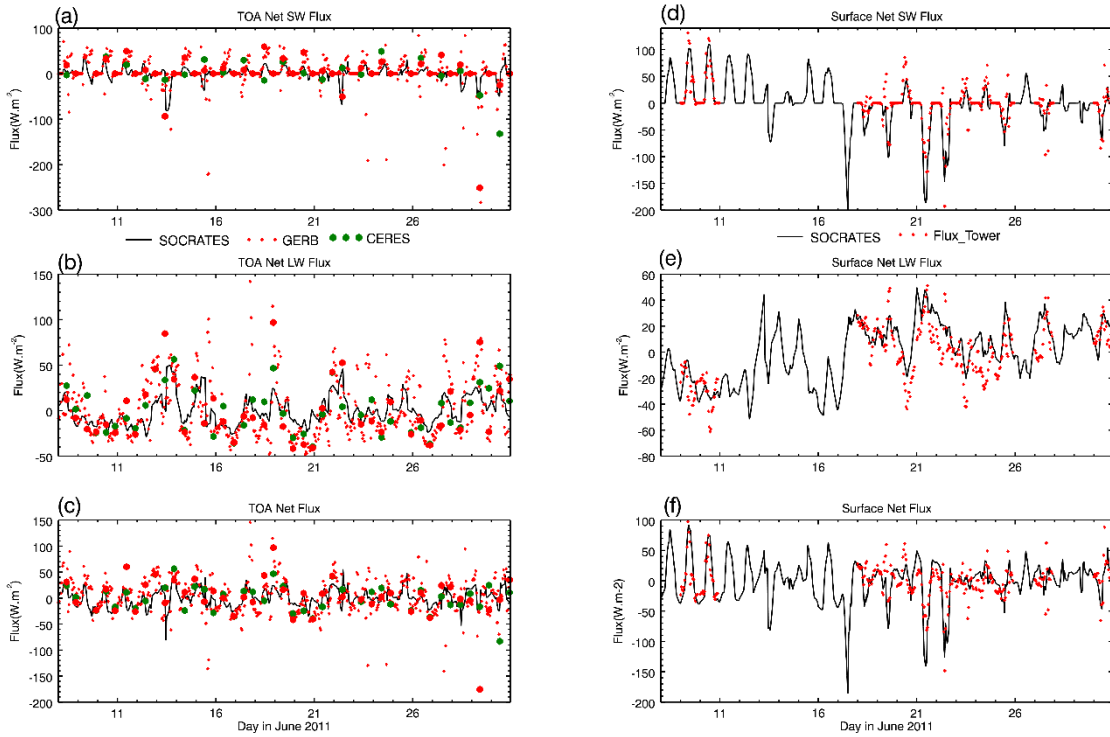
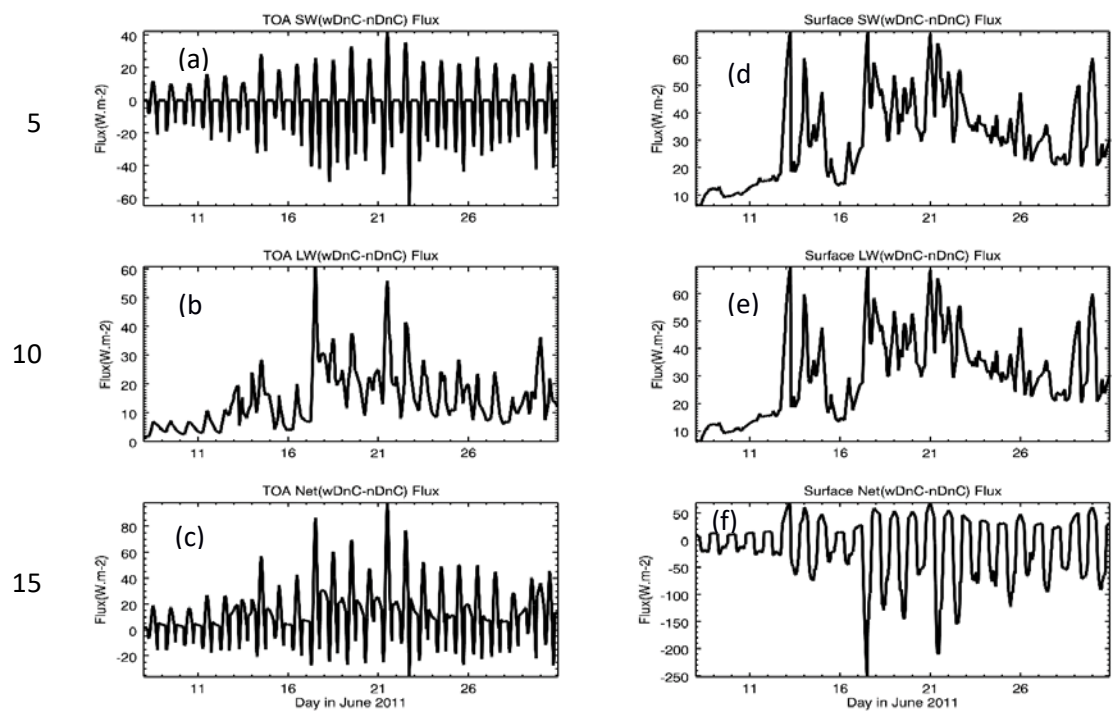


Figure S1. Same as fig. 6 but for anomalies



5

Figure S2. Same as fig 9 but for anomalies



20 Figure S3 DRE due to Dust: time series of TOA shortwave (a), longwave (b), net (c) and surface shortwave (d) longwave (e) and net (f) wdnC-nDnC flux